Studii şi Cercetări Ştiinţifice 2015, **16** (3), pp. 215 - 227
Chimie şi Inginerie Chimică, Biotehnologii, Industrie Alimentară

Scientific Study & Research
Chemistry & Chemical Engineering, Biotechnology, Food Industry *ISSN 1582-540X*

ORIGINAL RESEARCH PAPER

RADICAL QUENCHING OF METHANE-AIR PREMIXED FLAME IN MICROREACTORS USING DETAILED CHEMICAL KINETICS

Junjie Chen*, Deguang Xu

Henan Polytechnic University, School of Mechanical and Power Engineering, 454000, Jiaozuo, China

*Corresponding author: comcjj@163.com

Received: July, 18, 2015
Accepted: September, 04, 2015

Abstract: The steady hetero-/homogeneous combustion of lean methane-air mixtures in plane channel-flow microreactors was investigated numerically to elucidate the effects of wall material and initial sticking coefficient on radical quenching. Simulations were performed with a two-dimensional numerical model employing detailed reaction mechanisms to examine the interaction between heterogeneous and homogeneous reactions on platinum, alumina, quartz and copper. Comparisons among wall materials revealed that the wall chemical effect plays a vital role in the distribution of OH* radical. Homogeneous reaction of methane over platinum is significantly inhibited due to the rapid depletion of reactants on catalytic surfaces, rather than the radical adsorption. The inhibition of radical quenching on the surface of alumina is most pronounced. As the microreactor is smaller than the critical dimension of 0.7 mm, the wall chemical effect on flame characteristics becomes of great importance.

Keywords: *micro-combustion, microreactor, radical adsorption, radical quenching, surface reaction*

INTRODUCTION

Micro-combustors are emerging as a powerful tool for the portable production of energy. Hydrocarbon fuels contain a significantly larger energy density than traditional Li-ion type batteries (40 vs 0.5 $mJ \cdot kg^{-1}$) that are currently used in cellular phones, laptops, and other portable electronics devices [1]. The small scales in micro-combustors lead to lower combustion temperatures because of enhanced heat-transfer coefficients. Recent experiments [2] have demonstrated that micro-combustors could possibly reduce the gas-phase production of NO. Finally, micro-combustors can also serve as efficient sources of heat for endothermic reactions, such as ammonia decomposition and steam reforming, in integrated micro-chemical systems for the production of synthesis gas and hydrogen for fuel cell applications [3].

Sustaining stable combustion at the micro-scale is challenging because of large heat losses caused by the large surface-to-volume ratios of microreactors [4]. Homogeneous flames in reactors with sub-millimeter gap sizes [5] require careful materials treatment to minimize radical and thermal quenching; however, they still exhibit high temperatures that exceed the maximum operating temperatures of most materials of construction, compromising materials lifetime [6]. In contrast with homogeneous combustion, catalytic combustion (*i.e.*, heterogeneous combustion), which is typically avoided at large-scales, overcomes aforementioned problems, and allows high conversion efficiency at the micro-scale [7]. However, development of micro-structured reactors for energy productions and combustion applications is not a trivial matter.

Another concern for micro-combustion is radical quenching on the system walls. This quenching behavior is because of the removal of the active radicals from the reaction region by diffusion to the wall surface [8]. The heterogeneous reaction including radical adsorption at the surface bare sites, recombination, and desorption of recombined molecules becomes prevalent near the wall. When the removal of radicals is overly activated, flame is quenched even when the heat loss to the wall is insignificant. The radical quenching is more pronounced at high wall temperature where surface heat loss is small, because the heterogeneous reaction becomes dominant at high temperature. Radical quenching is also affected by the surface properties and treatment method for defect removal [9].

Aghalayam *et al.* [10] simulated the role of radical quenching in autothermal, ignition and extinction behavior of premixed hydrogen-air flames impinging on a flat surface, using surface radical recombination reactions and detailed homogeneous chemistry. The results showed that, under some conditions, the thermal feedback from the radical recombination renders the flame more stable, and results in a higher wall heat flux as compared with an inert surface. Raimondeau *et al.* [11] simulated flame propagation of methane-air in microchannels micro-flames, using detailed gas-phase chemistry and multicomponent transport, radical recombination at wall surfaces, heat loss through the wall, and possible temperature discontinuity at the wall. They found that the radical quenching and near-entrance heat loss are key factors for controlling flame propagation in micro-channels. Yang *et al.* [12] examined the effect of wall temperature and material on radical quenching of a premixed methane-air flame between two parallel walls, using a two-dimensional slit burner. They showed that the quenching distance reduces with increasing chemisorbed oxygen composition or wall temperature. Miesse *et al.* [13] investigated the dependence of wall materials and temperature on quenching

distance. They found that quenching distance strongly depends on the wall materials at wall temperature near 1273 K, while it does not dependent on wall materials when the wall temperature is below 500 K. Kim *et al.* [14] investigated experimentally the effects of surface characteristics and wall temperature on flame quenching of methane in two-dimensional slit micro-combustors to understand the physical mechanisms involving the heterogeneous radical recombination processes. The results showed that the quenching distances are independent of the surface property such as impurities, grain boundary, or oxygen vacancy at low temperatures; while the surface property strongly affect the quenching distance at high temperatures, indicating that radical removal on the wall plays a vital role in quenching process. Bai *et al.* [15] performed theoretical analyses on flame propagation in microreactors with emphasis on both radical and thermal quenching mechanisms. The results showed that the radical quenching effect becomes stronger at lower cross-over temperature and/or higher wall temperature; both the kinetic and thermal quenching limits are significantly extended with increasing wall temperature; flame extinction occurs with decreasing reactor dimension because of kinetic and/or thermal quenching. Fan *et al.* [16] employed the phase-locked OH-PLIF and time-resolved chemiluminescence imaging techniques to investigate the flame temperature, flame velocity and flame structure in the oscillation process for detailed discussion of the flame quenching and propagation. They found that, at high temperatures, radical quenching existed even on the quartz wall. Kizaki *et al.* [8] numerically and experimentally investigated the effect of radical quenching on methane-air flames to examine the quantitative effect of radical quenching on the homogeneous reaction, using a micro flow reactor with a controlled temperature profile. They found that the effect of radical quenching can be negligible at atmospheric pressure but it become strong at lower pressures.

However, the role of wall materials in radical quenching is not well understood, furthermore, the interaction between heterogeneous and homogeneous reactions still remains unclear. The main objectives are to elucidate the effect of wall materials and initial sticking coefficients on radical quenching of methane-air flames in microreactors, and to examine the interaction between heterogeneous and homogeneous reactions, using detailed homogeneous and heterogeneous chemical reaction schemes. Platinum, alumina, quartz and copper are chosen as the wall materials.

NUMERICAL MODELS AND SIMULATION APPROACH

Geometric model

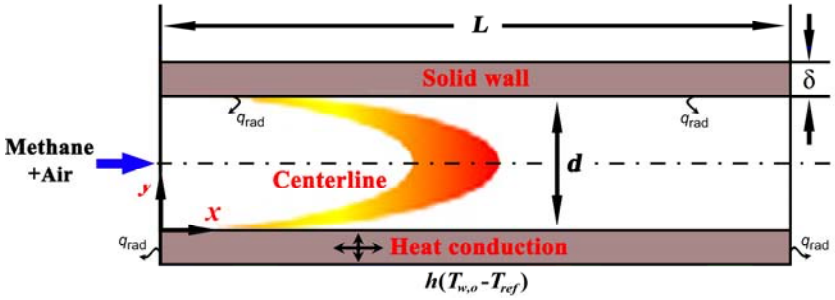

Figure 1. *Schematic diagram of the simulated microreactor*

The schematic diagram of the simulated microreactor is depicted in Figure 1. The configuration consists of a channel flow established between two parallel, infinitely wide plates, with a length L = 10.0 mm and a wall thickness δ = 0.4 mm. The plates are separated by a gap size of d = 2.0 mm. The wall materials of microreactors are platinum, quartz, alumina and copper, respectively. Their properties are given in Table 1. Methane-air mixtures are supplied into the reactor. The inlet mixture is at room temperature and at atmospheric pressure. Hereafter, x and y denote the streamwise and the wall-normal directions, respectively.

Table 1. *The properties of four wall materials*

Material	**Density [kg·m^{-3}]**	**Specific heat capacity [J·kg^{-1}·K^{-1}]**	**Thermal conductivity [W·m^{-1}·K^{-1}]**	**Thermal diffusion [m^2·s^{-1}]**
Platinum	21450	135	72	2.49×10^{-5}
Quartz	2500	890	0.7	3.15×10^{-7}
Alumina	3940	37	32	2.20×10^{-4}
Copper	8978	386	387	1.12×10^{-4}

Mathematical model

The reacting gas flow path and the characteristic length of the combustion chamber is still sufficiently larger than the molecular mean-free path of the air and other gases flowing through the micro-scale systems. Therefore, the fluid media can be reasonably considered as continuum in this work, and the Navier-Stokes equation was solved for the fluid domain. FLUENT-Kinetics [17] coupled with CHEMKIN [18 – 20] were used to simulate the premixed reacting flow and the interaction between homogeneous and heterogeneous reactions. The laminar-finite-rate model is adopted to consider the interaction between combustion and flow. The governing equations for laminar, steady and reactive gas flow with hetero-/homogeneous reaction are shown below:
Continuity equation:

$$\frac{\partial(\rho v_x)}{\partial x}+\frac{\partial(\rho v_y)}{\partial y}=0 \tag{1}$$

Momentum equation:

$$\frac{\partial(\rho v_x v_x)}{\partial x}+\frac{\partial(\rho v_x v_y)}{\partial y}=-\frac{\partial p}{\partial x}+\frac{\partial \tau_{xx}}{\partial x}+\frac{\partial \tau_{xy}}{\partial y} \tag{2}$$

$$\frac{\partial(\rho v_y v_x)}{\partial x}+\frac{\partial(\rho v_y v_y)}{\partial y}=-\frac{\partial p}{\partial y}+\frac{\partial \tau_{yx}}{\partial x}+\frac{\partial \tau_{yy}}{\partial y} \tag{3}$$

Energy equation:

$$\frac{\partial(\rho v_x h)}{\partial x}+\frac{\partial(\rho v_y h)}{\partial y}=\frac{\partial(k_f \partial T)}{\partial x^2}+\frac{\partial(k_f \partial T)}{\partial y^2}+\sum_i\left[\frac{\partial}{\partial x}\left(h_i\rho D_{i,m}\frac{\partial Y_i}{\partial x}\right)+\frac{\partial}{\partial y}\left(h_i\rho D_{i,m}\frac{\partial Y_i}{\partial y}\right)\right]-\sum_i h_i R_i \tag{4}$$

Species equation:

$$\frac{\partial(\rho Y_i v_x)}{\partial x}+\frac{\partial(\rho Y_i v_y)}{\partial y}=-\left[\frac{\partial}{\partial x}\left(\rho D_{i,m}\frac{\partial Y_i}{\partial x}\right)+\frac{\partial}{\partial y}\left(\rho D_{i,m}\frac{\partial Y_i}{\partial y}\right)\right]+R_i \tag{5}$$

where ρ, v, p, τ and T denote the density, velocity, pressure, shear stress and temperature, respectively; h_i is the enthalpy of the ith species; k_f is the thermal conductivity of fluid; Y_i, R_i and $D_{i,m}$ denote the mass fraction, the generation or consumption rate, and the mass diffusivity of the ith species.
Since heat transfer along the wall significantly affects the flame stability [21 – 23], heat transfer along the wall is considered in this model. The appropriate energy equation for the solid phase is given as follow:

$$\frac{\partial\left(k_s \partial T\right)}{\partial x^2}+\frac{\partial\left(k_s \partial T\right)}{\partial y^2}=0 \tag{6}$$

where k_s [$W \cdot m^{-1} \cdot K^{-1}$] denotes the thermal conductivity of solid wall.

Chemical kinetics

Detailed chemistry kinetics schemes are employed in both homogeneous and heterogeneous reactions. The oxidation of methane over platinum was described by the detailed scheme of Deutschmann *et al.* [24], which consists of 11 surface species and 24 elementary reactions. For other wall materials including quartz, alumina and copper, the radical quenching mechanism (shown in Table 2) proposed by Raimondeau *et al.* [11] is employed, consists of 5 surface species and 10 elementary reactions. In their radical quenching model, OH, O, H and CH_3 radicals play a significant role in ignition and extinction of methane-air [25, 26], and they adsorbed and desorbed on the surface and recombined to form the stable gas-phase species (H_2, O_2, H_2O, CH_4 and C_2H_6).

Table 2. *Radical quenching mechanism along with kinetic parameters*

Reactions	**pre-exponential [s^{-1}] or Sticking Coefficient**
$CH_3 + M^* \rightarrow CH_3^* + M$	0-1
$H + M^* \rightarrow H^* + M$	0-1
$OH + M^* \rightarrow OH^* + M$	0-1
$O + M^* \rightarrow O^* + M$	0-1
$2CH_3^* + 2\ M \rightarrow C_2H_6 + 2\ M^*$	10^{13}
$2H^* + 2\ M \rightarrow H_2 + 2\ M^*$	10^{13}
$2OH^* + M \rightarrow H_2O + O^* + M^*$	10^{13}
$2O^* + 2\ M \rightarrow O_2 + 2\ M^*$	10^{13}
$CH_3^* + H^* + 2\ M \rightarrow CH_4 + 2\ M^*$	10^{13}
$OH^* + H^* + 2\ M \rightarrow H_2O + 2\ M^*$	10^{13}

The rate of radical adsorption based on the Langmuir adsorption model is expressed by:

$$r_{ad}=\frac{p}{[s]\cdot\sqrt{2\pi MRT}}\cdot\left(1-\theta\right)\cdot s_0 \tag{7}$$

where p, $[s]$, M, R, θ and S_0 are partial pressure of the radical over the surface, concentration of free sites, molecular weight, ideal gas constant, fractional coverage of the surface and initial sticking coefficient of the radical, respectively. The concentrations of free sites are estimated from the distance between the neighboring

molecules on the wall surface, and are 2.706×10^{-9} (platinum) [24], 1.314×10^{-9} (quartz), 1.360×10^{-9} (alumina) and 3.153×10^{-9} (copper) mol·cm^{-2}, respectively.

Computation scheme

The boundary conditions used in this model are as follows. At the inlet, a fixed, flat velocity profile is used. At the exit, a fixed pressure is specified and far-field conditions are imposed for the rest of the variables, namely, zero diffusive flux of energy or species normal to the exit. In the bulk of the wall, the two-dimensional energy equation is solved. Symmetry boundary conditions are employed at the centerline between the two plates. The fluid density is calculated using the ideal gas law. The fluid thermal conductivity, specific heat, and viscosity are calculated from a mass fraction weighted average of species properties, and the species specific heat is calculated using a piecewise polynomial fit of temperature. The solid and fluid phases are linked with coupled interface. The convection and thermal radiation boundary conditions are employed at the outer wall surfaces. The discrete ordinates (DO) model is used to consider the effect of interior surface to surface radiation. The heat flux between solid wall and fluid is computed using the Fourier's law, and continuity in heat flux and temperature is ensured. Note that all the two-dimensional internal heat transfer within the solid and the fluid are calculated explicitly with the two-dimensional elliptic models without any further simplifications. On the wall, the mass fluxes corresponding to the surface reaction are defined and no-slip boundary conditions are imposed.

Uniform node spacing of 5.0 μm is utilized for all scenarios analyzed. Different mesh size has been tested to ensure grid-independence in computations. In prior to the productive run, dependency of the grid is carefully evaluated and the present grid is found to be fine enough. The equations of continuity, momentum, energy, and species are discretized with the finite-difference method. The thermal properties are computed using the CHEMKIN thermodynamic database and the transport properties are computed using CHEMKIN gas-phase transport database [20]. A second-order upwind difference scheme is used to discretize the governing equations and the SIMPLE algorithm is used to deal with the pressure-velocity coupling. To solve the conservation equations, a segregated solution solver with an under-relaxation method is used. The segregated solver first solves the momentum equations, then solves the continuity equation, and updates the pressure and mass flow rate. The energy and species equations are subsequently solved and convergence is checked. The simulation convergence is judged upon the residuals of the whole governing equations. The convergence criteria for the scaled residuals are set to be 1.0×10^{-5} for continuity, 1.0×10^{-6} for velocity, 1.0×10^{-7} for energy and 1.0×10^{-8} for species concentration.

The simulations are performed on a Beowulf cluster consisting of 8 × Xeon E7-8837 processors and 256 GB of RAM. When parallel processing is used, the message passing interface (MPI) is used to transmit information between nodes. In order to achieve convergence along with compute extinction points, natural parameter continuation is implemented. The computation time of each simulation varied between a few hours and several days, depending on the initial guess and the difficulty of the problem.

RESULTS AND DISCUSSION

Surface activity of platinum

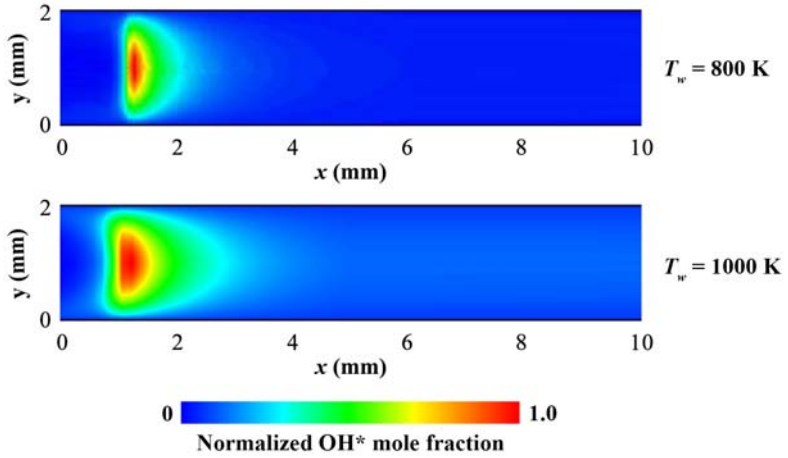

Figure 2. *The contours of normalized OH* mole fraction at different wall temperatures. The fuel is methane (φ = 0.8) and the wall material is platinum. The inlet temperature T_{in} and the inlet velocity V_{in} are 300 K and 2.0 $m{\cdot}s^{-1}$, respectively*

Figure 2 shows the contours of normalized OH* mole fraction by its maxima in platinum microreactor at different wall temperatures. The wall temperature T_w is kept constant and the equivalence ratio of methane-air mixtures is 0.8. Due to the thermal quenching effect, the OH* concentration near the platinum surfaces is very low and increases with the wall temperature. Figure 3 shows the wall-normal distributions of normalized OH* mole fraction near the platinum surfaces. Note that the OH* concentration becomes maximum at these streamwise positions (1.2 and 1.0 mm). The wall effect on OH* distribution is negligibly small at y = 1.6 mm, but the OH* concentration is monotonically decreased toward the platinum wall at y = 1.6-2.0 mm. This behavior shows that the thermal effect on the wall can be well represented by using the present model. Note that the simulation results are represented at these streamwise positions (1.2 and 1.0 mm) of maximum OH* concentration hereafter.

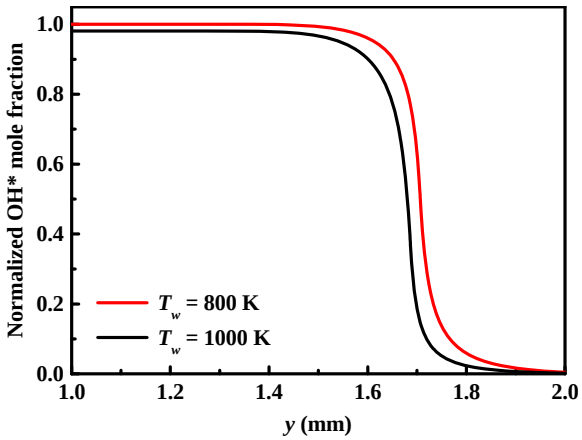

Figure 3. *Wall-normal distributions of normalized OH* mole fraction near the platinum surfaces at x = 1.2 mm (T_w = 800 K) and x = 1.0 mm (T_w = 1000 K)*

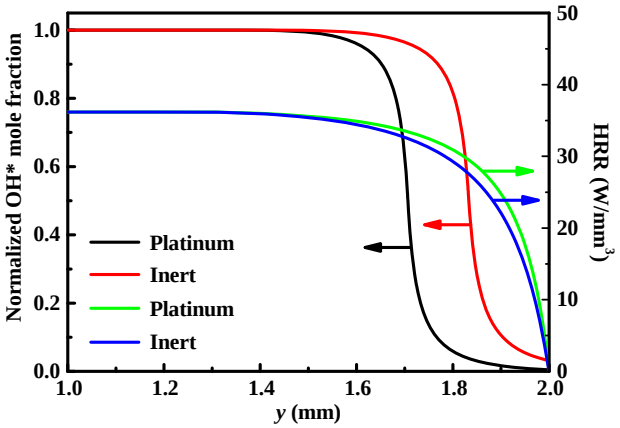

Figure 4. *Wall-normal distributions of normalized OH* mole fraction and heat release rate (HRR) on the platinum and inert surfaces at x = 1.0 mm (T_w = 1000 K)*

Figure 4 shows the wall-normal distributions of normalized OH* mole fraction and heat release rate on the platinum and inert surfaces at x = 1.0 mm. With the surface reaction on platinum, both the OH* mole fraction x_{OH} and the heat release rate are decreased at y = 1.6 - 2.0 mm. Under this condition, the heat generation in catalytic microreactors is decreased by approximately 2.0 %.

Figure 5 shows the streamwise distributions of methane and oxygen concentrations near the platinum and inert surfaces at y = 0.02 mm. Both methane and oxygen concentrations near the platinum surface are decreased dramatically as compare with the inert surface. This behavior is due to the rapid depletion of methane and oxygen on platinum by the surface catalytic reaction, resulting in the suppression of homogeneous flame near the platinum surface. The effect of radical adsorption on homogeneous flame is also examined by using separate simulation coupling surface catalytic reaction mechanism excluding the adsorption of H*, O*, and OH* radicals on the platinum surface. However, simulation results show that the homogeneous flame structure is almost unchanged, indicating that the homogeneous reaction of methane over platinum is significantly inhibited due to the rapid depletion of reactants on catalytic surfaces, rather than the radical adsorption.

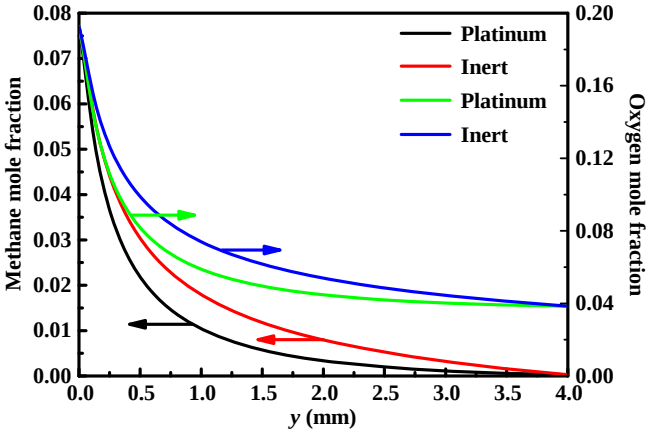

Figure 5. *Streamwise distributions of methane and oxygen concentrations near the platinum and inert surfaces at y = 0.02 mm (T_w = 1000 K)*

Surface activity of quartz, alumina and copper

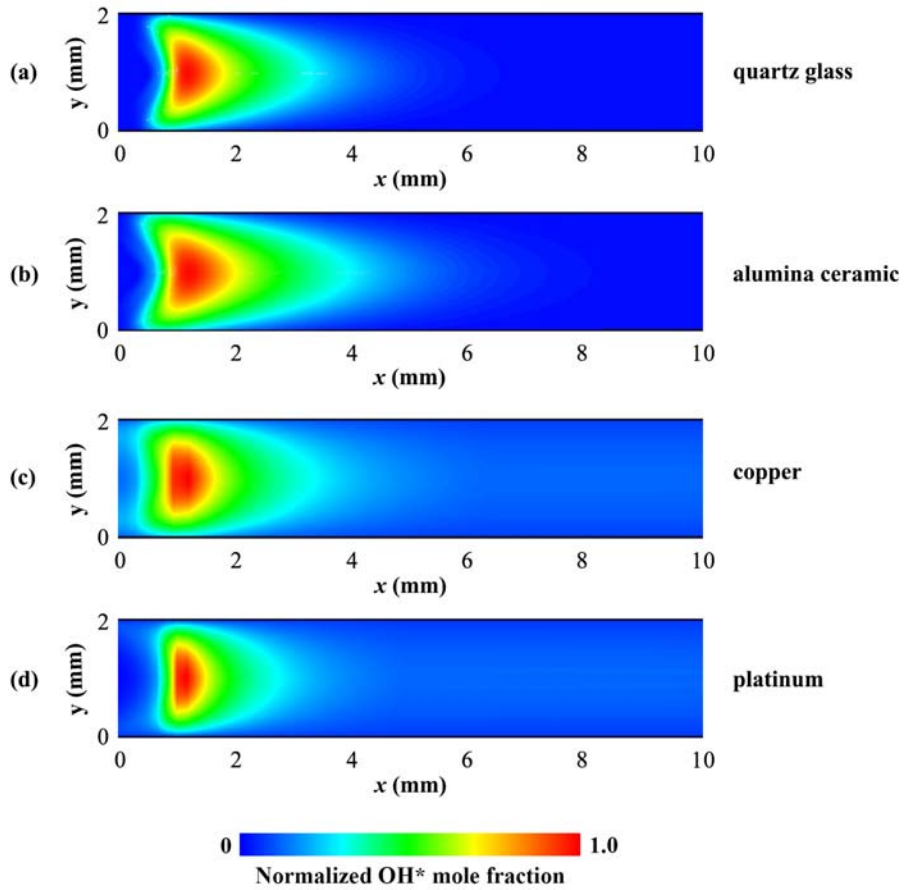

Figure 6. *The contours of normalized OH* mole fraction at T_w = 1000 K. The fuel is methane (φ = 0.8) and the wall materials are quartz, alumina, copper and platinum, respectively. The inlet temperature T_{in} and the inlet velocity V_{in} are 300 K and 2.0 m·s^{-1}, respectively*

Aside from platinum, it is important to understand the radical quenching behavior on the surface of other wall materials. Figure 6 shows the normalized OH* mole fraction for different wall materials (quartz, alumina, copper and platinum) at T_w = 1000 K. Wall chemical effect plays a crucial role in the distribution of OH* radical. It has the largest wall chemical effect on the surface of platinum, and the OH* concentration near the surface region (y = 0 - 0.02 mm) of platinum is the lowest as observed in Figure 6d. This behavior is due to the radical quenching that consists of radical adsorption, recombination, and desorption of recombined molecules.

Near the surface of quartz (generally identified as inert surface) as observed in Figure 6a, the OH* concentration is much increased. The distribution of OH* radical near the copper surface (Figure 6c) is slightly lower than quartz. This behavior is because copper has the part catalytic effect [27, 28]. However, the OH* concentration near the surface of alumina (Figure 6b) is much higher than quartz, indicating that radical quenching is the most inhibited on the surface of alumina.

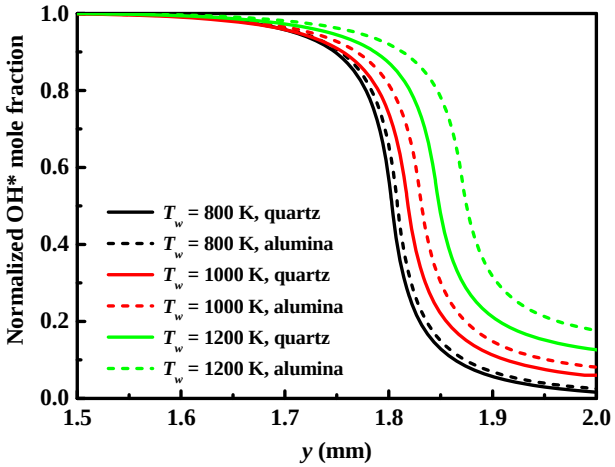

Figure 7. *Wall-normal distributions of normalized OH* mole fraction near the surfaces of quartz and alumina at x = 1.2 mm (T_w = 800 K), x = 1.0 mm (T_w = 1000 K) and x = 0.8 mm (T_w = 1200 K)*

The wall-normal distributions of normalized OH* mole fraction near the surfaces of quartz and alumina for different wall temperatures are shown in Figure 7. Note that the OH* concentration becomes maximum at these streamwise positions (1.2, 1.0 and 0.8 mm). At lower wall temperature (800 K), the effect of wall material on distribution of OH* concentration is very small. However, the OH* concentration at higher wall temperature (1200 K) is strongly dependent on wall material. This behavior is qualitatively consistent with the previous work of quenching distance by Miesse *et al.* [13], who used quartz, alumina, stainless steel, and cordierite ($Mg_2Al_4Si_5O_{18}$) as wall material, and found that the quenching distance strongly depended when the wall temperature is near 1273 K, while did not dependent on wall material when that is below 500 K.

Effect of initial sticking coefficient

Sticking coefficient S is the term used to describe the ratio of the number of adsorbate radicals that adsorb to wall surface to the total number of radicals that impinge upon that wall surface during the same period of time. The coefficient is a function of surface temperature, surface coverage and structural details as well as the kinetic energy of the impinging particles. The initial sticking coefficient is crucial for the radical quenching behavior because the quenching process is considered to be adsorption-limited [11, 13]. In the present work, the effect of initial sticking coefficient is evaluated through OH* concentration distribution and the profiles of surface site fraction.

Figure 8 shows the fraction of surface site obtained with initial sticking coefficient S_0 = 1.0, by which the radical adsorption is the most enhanced. The fractions of surface site for four surface species (H(s), OH(s), O(s), and CH_3(s)) are on the order of 10^{-4} although the sticking coefficient is 1.0. On the other hand, the remaining surface sites are unoccupied. It shows that the quenching process is limited by radical adsorption, and radical adsorption is dominant for wall chemical effect.

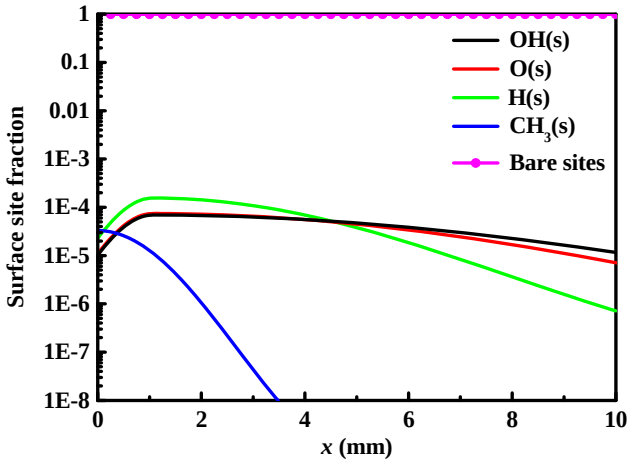

Figure 8. *The fraction of surface site obtained with initial sticking coefficient S_0 = 1.0 at T_w = 1000 K*

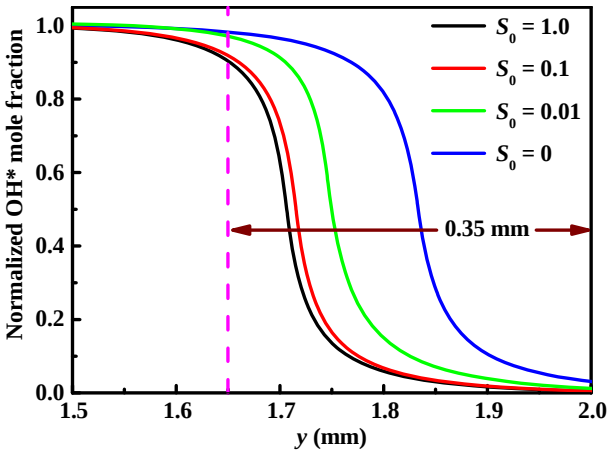

Figure 9. *Wall-normal distributions of normalized OH* mole fraction near the wall surface (y = 0.02 mm) with initial sticking coefficient S_0 = 1.0, 0.1, 0.01 and 0 at T_w = 1000 K*

Figure 9 shows the wall-normal distributions of normalized OH* mole fraction near the wall surface (y = 0.02 mm) with initial sticking coefficient S_0 = 1.0, 0.1, 0.01 and 0 (namely inert surface) at T_w = 1000 K. For initial sticking coefficients S_0 = 1.0 and 0.1, OH* concentration in the vicinity of the wall surface becomes closer to 0 compare with S_0 = 0.01 and 0 due to large quenching affinities. Note that the discrepancy of OH* distribution for different initial sticking coefficients becomes significant within 0.35 mm from the wall surface. Therefore, the wall chemical effect on flame characteristics becomes very important as the microreactor is smaller than 0.7 mm.

CONCLUSIONS

Radical quenching behaviors of methane-air flame in microreactors with various wall materials were conducted employing detailed reaction mechanisms to elucidate the interaction between heterogeneous and homogeneous reactions on the surfaces of

platinum, quartz, alumina and copper. It was also performed to estimate the effect of initial sticking coefficients associated with radical adsorption on radical quenching. Simulations indicate that the wall chemical effect plays a vital role in the distribution of OH* radical. Homogeneous reaction of methane over platinum is significantly inhibited due to the rapid depletion of reactants on catalytic surfaces, rather than the radical adsorption. Radical quenching on the surface of alumina is most inhibited. The initial sticking coefficient has a significant effect on the distribution of OH* radical within 0.35 mm from the wall surface. Consequently, as the microreactor is smaller than the critical dimension of 0.7 mm, the wall chemical effect on flame characteristics becomes of great importance.

ACKNOWLEDGMENTS

This work was supported by the National Natural Science Foundation of China (No. 51506048).

REFERENCES

1. Miyata, E., Fukushima, N., Naka, Y., Shimura, M., Tanahashi, M., Miyauchi, T.: Direct numerical simulation of micro combustion in a narrow circular channel with a detailed kinetic mechanism, *Proceedings of the Combustion Institute*, **2015**, **35** (3), 3421-3427;
2. Yang, W., Deng, C., Zhou, J., Liu, J., Wang, Y., Cen, K.: Experimental and numerical investigations of hydrogen-air premixed combustion in a converging-diverging micro tube, *International Journal of Hydrogen Energy*, **2014**, **39** (7), 3469-3476;
3. Stefanidis, G.D., Vlachos, D.G.: Intensification of steam reforming of natural gas: Choosing combustible fuel and reforming catalyst, *Chemical Engineering Science*, **2010**, **65** (1), 398-404;
4. Rana, U., Chakraborty, S., Som, S.K.: Thermodynamics of premixed combustion in a heat recirculating micro combustor, *Energy*, **2014**, **68**, 510-518;
5. Zimont, V.L.: Theoretical study of self-ignition and quenching limits in a catalytic micro-structured burner and their sensitivity analysis. *Chemical Engineering Science*, **2015**, **134**, 800-812;
6. Kaisare, N.S., Deshmukh, S.R., Vlachos, D.G.: Stability and performance of catalytic microreactors: Simulations of propane catalytic combustion on Pt, *Chemical Engineering Science*, **2008**, **63** (4), 1098-1116;
7. Yan, Y., Pan, W., Zhang, L., Tang, W., Chen, Y., L. Li.: Numerical study of the geometrical parameters on CH_4/air premixed combustion in heat recirculation micro-combustor, *Fuel*, **2015, 159**, 45-51;
8. Kizaki, Y., Nakamura, H., Tezuka, T., Hasegawa, S., Maruta, K.: Effect of radical quenching on CH_4/air flames in a micro flow reactor with a controlled temperature profile, *Proceedings of the Combustion Institute*, **2015**, **35** (3), 3389-3396;
9. Choi, W., Kwon, S., Shin, H.D.: Combustion characteristics of hydrogen-air premixed gas in a sub-millimeter scale catalytic combustor, *International Journal of Hydrogen Energy*, **2008**, **33** (9), 2400-2408;
10. Aghalayam, P., Bui, P.-A., Vlachos, D.G.: The role of radical wall quenching in flame stability and wall heat flux: hydrogen-air mixtures, *Combustion Theory and Modelling*, **1998**, **2** (4), 515-530;
11. Raimondeau, S., Norton, D.G., Vlachos, D.G., Masel, R.I.: Modeling of high-temperature microburners, *Proceedings of the Combustion Institute*, **2002**, **29** (1), 901-907;
12. Yang, H., Feng, Y., Wang, X., Jiang, L., Zhao, D., Yamashita, H.: A surface analysis-based investigation of the effect of wall materials on flame quenching, *Combustion Science and Technology*, **2011**, **183** (5), 444-458;

13. Miesse, C.M., Masel, R.I., Jensen, C.D., Shannon, M.A., Short, M.: Submillimeter-scale combustion, *AIChE Journal*, **2004**, **50** (12), 3206-3214;
14. Kim, K.T., Leeb D.H., Kwon, S.: Effects of thermal and chemical surface-flame interaction on flame quenching, *Combustion and Flame*, **2006**, **146** (1-2), 19-28;
15. Bai, B., Chen, Z., Zhang, H., Chen, S.: Flame propagation in a tube with wall quenching of radicals, *Combustion and Flame*, **2013**, **160** (12), 2810-2819;
16. Fan, Y., Suzuki, Y., Kasagi, N.: Quenching mechanism study of oscillating flame in micro channels using phase-locked OH-PLIF, *Proceedings of the Combustion Institute*, **2011**, **33** (2), 3267-3273;
17. *Fluent 6.3 user's guide*, Lebanon, New Hampshire: Fluent Inc., **2006**;
18. Kee, R.J., Rupley, F.M., Meeks, E., Miller, J.A.: *Chemkin: a Fortran chemical kinetics package for the analysis of gas-phase chemical kinetics*, Report No. SAND96-8216, Technical Report, Sandia National Laboratories, **1996**;
19. Coltrin, M.E., Kee, R.J., Rupley, F.M., Meeks, E.: *Surface Chemkin: a Fortran package for analyzing heterogeneous chemical kinetics at a solid surface/gas-phase interface*, Report No. SAND96-8217, Technical Report, Sandia National Laboratories, **1996**;
20. Kee, R.J., Dixon-Lewis, G., Warnatz, J., Coltrin, M.E., Miller, J.A.: *A Fortran computer code package for the evaluation of gas-phase multicomponent transport properties*, Report No. SAND86-8246, Technical Report, Sandia National Laboratories, **1996**;
21. Schultze, M., Mantzaras, J., Grygier, F., Bombach, R.: Hetero-/homogeneous combustion of syngas mixtures over platinum at fuel-rich stoichiometries and pressures up to 14 bar, *Proceedings of the Combustion Institute*, **2015**, **35** (2), 2223-2231;
22. Cuoci, A., Frassoldati, A., Faravelli, T., Ranzi, E.: Extinction of laminar, premixed, counter-flow methane/air flames under unsteady conditions: Effect of H_2 addition, *Chemical Engineering Science*, **2013**, **93**, 266-276;
23. Wan, J., Fan, A., Yao, H., W. Liu.: Effect of thermal conductivity of solid wall on combustion efficiency of a micro-combustor with cavities, *Energy Conversion and Management*, **2015**, **96**, 605-612;
24. Deutschmann, O., Maier, L.I., Riedel, U., Stroemman, A.H., Dibble, R.W.: Hydrogen assisted catalytic combustion of methane on platinum, *Catalysis Today*, **2000**, **59** (1-2), 141-150;
25. Vlachos, D.G., Schmidt, L.D., Aris, R.: Ignition and extinction of flames near surfaces: combustion of CH_4 in air, *AIChE Journal*, **1994**, **40** (6), 1005-1017;
26. Vlachos, D.G., Schmidt, L.D., Aris, R.: Ignition and extinction of flames near surfaces: Combustion of H_2 in air, *Combustion and Flame*, **1993**, **95** (3), 313-335;
27. Li, J., Zhang, R., Wang, B.: Influence of the hydroxylation of γ-Al_2O_3 surfaces on the stability and growth of Cu for Cu/γ-Al_2O_3 catalyst: A DFT study, *Applied Surface Science*, **2013**, **270**, 728-736;
28. Zhang, R., Sun, X., Wang, B.: Insight into the Preference Mechanism of CH_x (x = 1-3) and C-C Chain Formation Involved in C_2 Oxygenate Formation from Syngas on the Cu (110) Surface, *The Journal of Physical Chemistry C*, **2013**, **117** (13), 6594-6606.